frontiers | Frontiers in Mechanical Engineering

TYPE Original Research
PUBLISHED 14 June 2024
DOI 10.3389/fmech.2024.1393959

OPEN ACCESS

EDITED BY
Kanak Kalita,
Vel Tech Dr. RR & Dr. SR Technical University, India

REVIEWED BY
Satyanarayan,
Kumamoto University, Japan
Manoj Kumar R.,
VIT University, India
Ashutosh Agrawal,
University of Hasselt, Belgium
Neeraj Bhoo,
Banasthali University, India
Arun Kumar Sharma,
Sangam University, India

*CORRESPONDENCE
Dasappa Ramesh,
rameshd@ssit.edu.in
Vishwanatha H. M.,
vishwanatha.hm@manipal.edu

RECEIVED 29 February 2024
ACCEPTED 13 May 2024
PUBLISHED 14 June 2024

CITATION
Pattar J, Ramesh D, Malghan RL, Kumar A, Kumar P and H. M. V (2024), Investigation of AA6063-based metal–matrix composites reinforced with TiO_2 dispersoids through digitally assisted techniques for mechanical, tribological, and microstructural characterizations. *Front. Mech. Eng* 10:1393959. doi: 10.3389/fmech.2024.1393959

Investigation of AA6063-based metal–matrix composites reinforced with TiO_2 dispersoids through digitally assisted techniques for mechanical, tribological, and microstructural characterizations

Jagannath Pattar[1,2], Dasappa Ramesh[1]*, Rashmi Laxmikant Malghan[3], Ajay Kumar[4], Pawan Kumar[5] and Vishwanatha H. M.[6]*

[1]Department of Mechanical Engineering, SSIT Tumkur, Sri Siddhartha Academy of Higher Education, Tumkur, India, [2]Department of Mechanical Engineering, Madanapalle Institute of Technology and Science, Madanapalle, India, [3]Department of Data Science & Computer Applications, Manipal Institute of Technology, Manipal Academy of Higher Education, Manipal, India, [4]Department of Mechanical Engineering, School of Engineering and Technology, JECRC University, Jaipur, India, [5]Joint Institute of Mechanical Engineering of the National Academy of Sciences of Belarus, Minsk, Belarus, [6]Department of Mechanical and Industrial Engineering, Manipal Institute of Technology, Manipal Academy of Higher Education, Manipal, India

Aluminum metal–matrix composites (AMMCs) were prepared by dispersing TiO_2 dispersoids of different volume fractions into an AA6063 matrix via stir casting and subjected to process–structure correlation studies. Four different samples based on weight ratio were considered herein: 99Al-1TiO_2, 97Al-3TiO_2, 95Al-5TiO_2, and the as-received AA6063. Their mechanical properties namely, microhardness, tensile strength, and tribological behavior, were determined. In addition, the microstructure of the samples was also analysed. It was observed that the addition of 5% TiO_2 particles enabled the AA6063 matrix to accommodate a higher strain energy while providing the required driving force to generate dislocations and substructures. Therefore, considering the plastic deformation, the ultimate tensile strength (σ_{ut}) increased gradually with the addition of TiO_2 (in weight%). The flow curves of the 95Al-5TiO_2 sample showed the highest value of σ_{ut}, whereas the as-received AA6063 matrix exhibited the lowest value. For linear elastic deformation, AA6063 showed the lowest yield strength (σ_{ys}) as compared to the AMMC samples for all TiO_2 weight% values; however, the variation in σ_{ys} among the AMMC samples was minimal. The microhardness of the samples increased gradually with the addition of TiO_2, and the percentage reduction in area at the fracture was largest for 95Al-5TiO_2. The Taguchi's L9 array and variance analysis of the process parameters indicated that the material wear was largely affected by the normal load, followed by weight% of TiO_2 and sliding

Abbreviations: AMMC, aluminum metal–matrix composite; ANOVA, analysis of variance; EDX, energy-dispersive X-ray spectroscopy; GB, grain boundary; MMC, metal–matrix composite; OM, optical microscopy; SEM, scanning electron microscopy.

speed. Wear surface characteristics, such as microvoids, delamination, microcracks, and wear debris, were qualitatively observed in all the AMMC samples. The overall strength improvement was attributable to the effects of addition of the dispersoids. During melt solidification, the TiO_2 particles surpassed/pinned and hindered the grain growth, resulting in grain-size refinement.

KEYWORDS

aluminum metal–matrix composite, ultimate tensile strength, microhardness, yield strength, wear rate, precipitation, grain refinement

1 Introduction

Aluminum metal–matrix composite (AMMC) is a form of metal–matrix composite (MMC) in which aluminum is used as the matrix (Dey et al., 2021; Reddy et al., 2022). An MMC is a composite made up of at least two constituent materials, one of which must be a metal (Reddy et al., 2022). AMMCs have attracted substantial attention in recent years owing to their excellent mechanical and thermal properties, which have enabled their use in various industrial applications (Mavhungu et al., 2017; Srivyas and Charoo, 2019). AMMCs contain an aluminum matrix reinforced with other carbide and oxide alloys that offer a unique blend of high strength, low density, and enhanced wear resistance (Pramanik, 2016). Among the various types of reinforcements, boron carbide (B_4C) and titanium dioxide (TiO_2) have exhibited remarkable potential for enhancing the mechanical, tribological, and microstructural properties of AMMCs (Veeresh Kumar et al., 2017). On the other hand, aluminum and its alloys, which are renowned for their lightweight characteristics and corrosion resistance, are extensively used as the matrix in MMCs for aerospace, automotive, and other high-performance engineering applications (Dutt et al., 2021; Kumar, 2022; Kumar and Verma, 2022). Among the aluminum alloys, AA6063 has been widely used owing to its excellent extrudability and formability. Scientists and researchers have explored the integration of ceramic reinforcements to attain further enhancement of the mechanical and tribological characteristics. The combination of B_4C and TiO_2 particles is a compelling method of creating hybrid MMCs with synergistically improved attributes. B_4C is known for its high hardness and enhanced wear resistance, whereas TiO_2 offers unique chemical and mechanical properties.

Subramanian et al. reported the use of Si_3N_4 and BN reinforcements to improve the hardness and tribological characteristics of Al7068-based AMMCs (Subramanian et al., 2021); increasing the Si_3N_4 content in this AMMC improved the wear resistance while decreasing the wear rate (WR) and coefficient of friction (COF). In addition to the tribological characteristics, Yunus et al. reported the microstructural properties by considering B_4C and graphite reinforcements, which impeded the dislocation movements and enhanced the material hardness, wear resistance, and microstructural as well as compressive properties (Yunus and Alfattani, 2023). In another work, Manoj Kumar et al. observed improved wear resistance of the Al6063-based AMMC upon reinforcement with fly ash and graphite (Manojkumar and Shanmuga Prakash, 2016). Minimized porosity showing wear resistance as well as predominantly abrasive and oxidative wear mechanisms at lower applied loads are also reported in other works (Chelladurai et al., 2021; Nandyala et al., 2023). In the context of mechanical properties, Ramesh et al. studied hybrid AMMCs and reported that the load transfer between the matrix and reinforcement as well as strain hardening effects were owed to the increased hardness (Ramesh et al., 2015). Shuvho et al. studied Al6063-based MMCs reinforced with Al_2O_3/SiC/TiO_2 and reported higher hardness, tensile strength, and yield strength compared to the pure Al6063 with increasing reinforcement (Shuvho et al., 2020). Shin et al. reported the interface reactions and their influences on the mechanical properties using TiO_2 nanoparticles as reinforcement; they noted that the higher chemical potential energy of the reinforcement induced dissolute formation of the interface layer and higher yield strength (Shin et al., 2014). Similarly, another study showed that aluminum oxide and TiO_2 reinforcement improved the impact strength of the AMMC with simultaneous amalgamation of the reinforcements (Ahamad et al., 2020). In the context of microstructural properties, the AMMC wear surface showed abrasion, oxidation, and delamination as the dominant wear mechanisms (Joshua et al., 2018). However, diminished mechanical and wear properties were obtained for TiO_2-based AMMCs at higher reinforcement weight% values owing to agglomeration of the reinforcement material (Alagarsamy and Ravichandran, 2019). A severely damaged machined subsurface with numerous geometrical defects and plastically deformed aluminum matrix was reported in another work (Kannan and Kishawy, 2006). The effects of particulate volume fraction and average size on alteration of the microhardness of the matrix were also investigated. Other types of composites and laminates prepared using different fabrication techniques have also been investigated by other researchers (Tyagi et al., 2021; Goyat et al., 2022; Singh et al., 2023; Kumar et al., 2024; Wagih et al., 2024). Bhoi et al. studied the mutual effects of ZnO nanorods and Y_2O_3 nanoparticles on the microstructural and mechanical responses of aluminum (Bhoi et al., 2022a); they reported that the enhanced material responses could be attributed to the uniform distribution of ZnO and Y_2O_3 in the hybrid composite material. In another similar work, they studied an aluminum-yttrium-oxide MMC synthesized by microwave hybrid sintering and reported enhanced nano hardness and elastic modulus (Bhoi et al., 2022b); the authors also synthesized a zinc-oxide-reinforced AMMC and noted a similar trend in the nanohardness, with marginal decrease of the elastic modulus (Kumar Bhoi et al., 2020).

Based on the above works, it is noted that the correlations between the microstructures and properties require further

TABLE 1 Weight-to-weight ratios of different samples.

Sample number	AA6063 (weight %)	TiO_2 (weight %)	Sample name
1	100	0	AA6063
2	99	1	99Al-1TiO_2
3	97	3	97Al-3TiO_2
4	95	5	95Al-5TiO_2

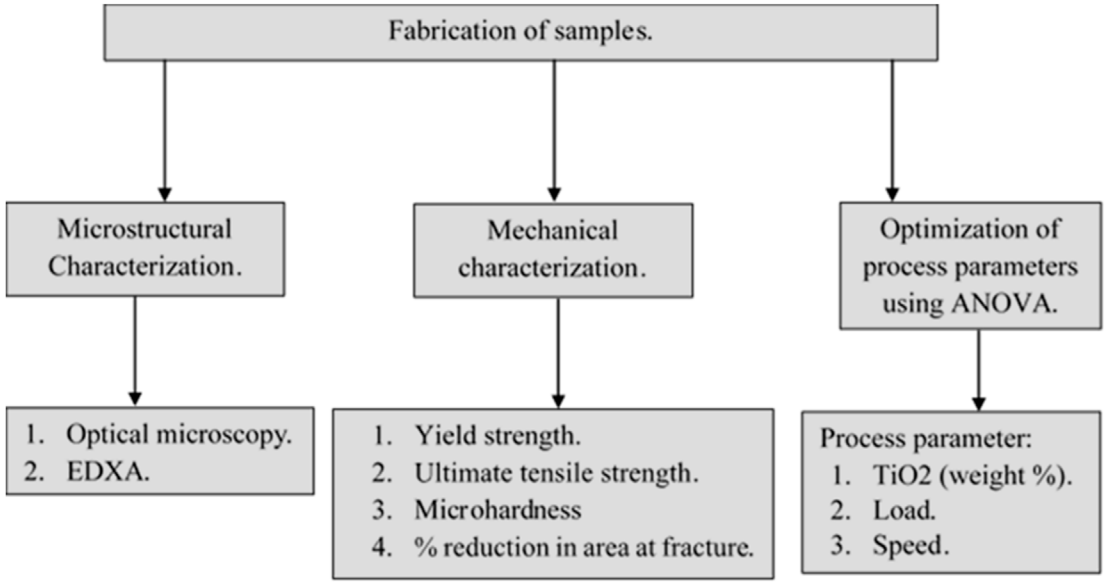

FIGURE 1
Flow diagram for the experimental procedures and characterizations.

insights upon consideration of the combined tribological and mechanical behaviors of AA6063-TiO_2. Therefore, in the present work, AA6063-TiO_2 AMMCs with varying reinforcement weight% values were fabricated via stir casting. There are various fabrication methods for AMMCs, such as powder metallurgy, diffusion bonding, infiltration, and squeeze casting; however, stir casting is the most common commercial method of producing Al-matrix composites out of these techniques, where the melt is actively stirred during solidification and mixing with the reinforcing phase (Hang, 2022). This method is simpler and more flexible than other fabrication methods; it is also suitable for near-net shape components and is relevant to large-volume production. The stirring process has some important advantages, including a wider selection of materials, better matrix–particle bonding, easier control of the matrix structure, and simpler and inexpensive processing (Arsha et al., 2022). The mechanical, tribological, and microstructural properties such as ultimate tensile strength, yield strength, percentage reduction in area at fracture, microhardness, WR, effect of wear force, grain refinement, and precipitation strengthening were studied using adequate characterization techniques. The results were finally compared, and the process parameters were optimized.

2 Materials and methodology

The material investigated in this study was AA6063 AMMC reinforced with TiO_2. Four different samples were prepared in accordance with the weight ratio as 99Al-1TiO_2, 97Al-3TiO_2, 95Al-5TiO_2, and as-received AA6063 and evaluated thereafter. The weight% values of the matrix and reinforcement are presented in Table 1.

The flow diagram for the experimental procedures and characterizations is shown in Figure 1. The samples were prepared by a stir-casting process. Stir casting is a liquid-state method of fabricating composite materials, in which a dispersed phase is mixed with a molten matrix metal via mechanical stirring (Nandyala et al., 2023); the liquid composite material is then cast using various casting methods. However, uniform distribution of the TiO_2 particles in the aluminum matrix was challenging owing to the wettability, porosity, and chemical reactions between the reinforcement material and matrix alloy (Alagarsamy and Ravichandran, 2019; Ahamad et al., 2020). Hence, a stirrer was used to disperse the TiO_2 particles in the alloy matrix. AA6063 was used as the matrix material and TiO_2 was used as the reinforcement. A zirconia crucible was used for melting as it possesses high resistance to thermal shock and wetting by

FIGURE 2
Samples used for tensile testing.

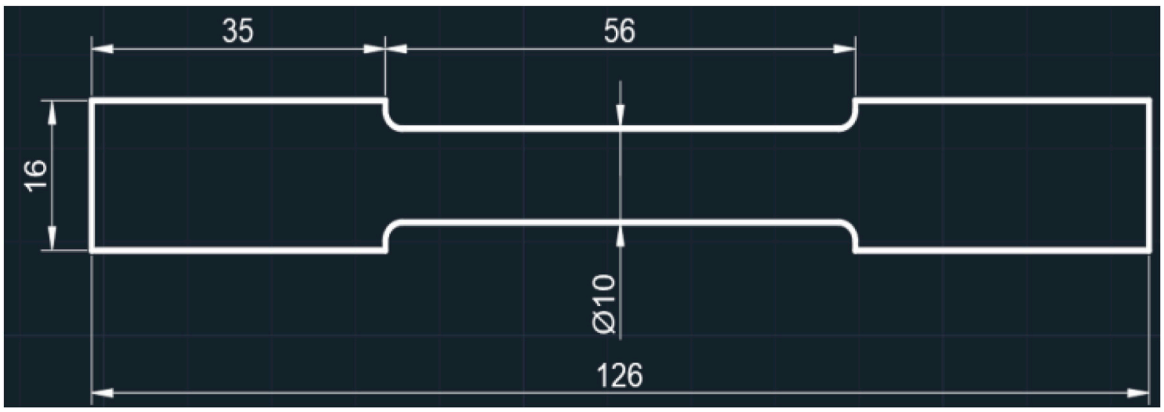

FIGURE 3
Dimensions of the samples used for the tensile tests; all dimensions are in mm.

molten metals, has low thermal expansion, and avoids carbon pickup. The crucible and reinforcements (in powder form) were preheated to a temperature of 400°C using an induction furnace to remove any moisture content as moisture affects the charge (matrix and reinforcement) reading and testing; the preheating of the reinforcement also enables better adhesion with the matrix, improves the heat insulation of the molten metal, and prevents temperature reduction.

The AA6063 ingots were heated to a temperature of 800°C, and the preheated reinforcement material was mechanically mixed with AA6063 simultaneously. The charge was melted using an induction furnace at a temperature of 830°C. The charge homogenization was achieved by the melt stirring at the rate of 550 rpm for 10 min. For the stirring process, three propeller blades were fixed on a shaft connected to the output shaft of an electric motor, and the height of the stirrer was adjustable through the lead screw power. The microhardness values of the samples were obtained using the FMV-1 Vickers microhardness testing apparatus at a load of 2 kg and dwell time of 15 s. The 136° pyramidal diamond indenter was used for the microhardness tests. The samples for this test were prepared by cutting them semiaxially using a waterjet cutting apparatus. The yield strength (σ_{ys}), ultimate tensile strength (σ_{ut}), fitted strain, and percentage reduction in area at fracture were calculated using a servohydraulic universal testing apparatus (INSTRON 8800). The tensile test specimens were prepared in accordance with the ASTM E8 standard (Kardak and Sinclair, 2020). The cylindrical samples with diameters of 10 mm and gauge lengths of 50 mm each were used to generate flow curves at room temperature; the test samples and sample dimensions are shown in Figures 2, 3, respectively. The samples were subjected to large-scale plastic deformations under a tensile load. The microstructural characterizations were performed via optical microscopy (OM), energy-dispersive X-ray spectroscopy (EDX, ESEM Quanta 200, FEI) attachment fitted to a scanning electron microscopy (SEM) device operated at a voltage of 20 kV in the high-current mode. The EDX samples were prepared by cutting the samples with a grinding machine and a diamond cutter. The mounted samples were then mechanically polished using emery papers with grit levels ranging from 100 to 500 µm, followed by cloth polishing using a TEGRAPOL polishing apparatus. The polishing grit were used in the size sequence of 9µ, 3µ, and 1µ for mechanical polishing.

The tribological studies were conducted in accordance with the Taguchi technique. The dry sliding wear tests were conducted

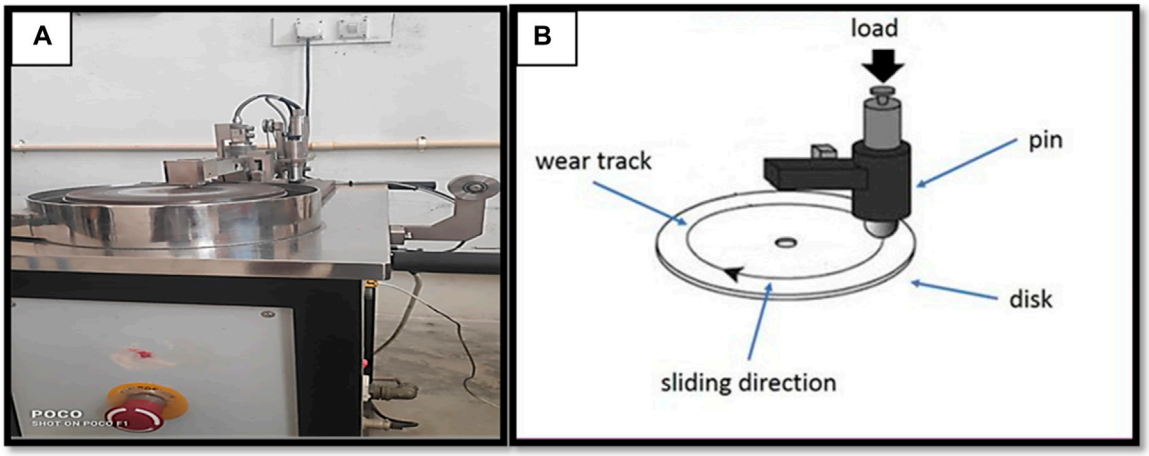

FIGURE 4
Pin-on-disc wear test **(A)** apparatus (model NTS-V01) along with **(B)** load and sliding directions.

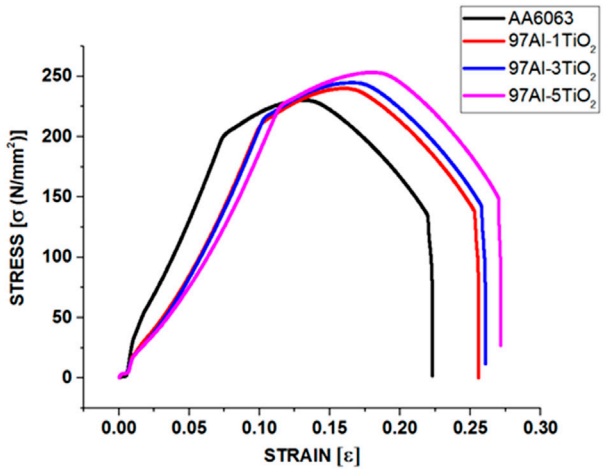

FIGURE 5
Flow curve of the AA6063, 99Al-1TiO_2, 97Al-3TiO_2, and 95Al-5TiO_2 samples.

using a pin-on-disc test setup as per ASTM G99-19 standards; the pin-on-disc test apparatus (NTS-V01) is shown in Figure 4A. The sliding direction in the circumferential plane and load in the axial direction are shown in Figure 4B. The sample pin was pressed against the steel disc, which was rotated at speeds of 1, 2, and 3 m/s. The hardness of the steel disc was 62 HRC, with a surface roughness of 0.5 µm. The sliding wear tests were conducted at room temperature. Before each test, the disc and samples were cleaned using acetone to eliminate possible experimental errors. The mass losses were determined using a mass balance (LF-225DR semimicro balance). All experimental trials were planned as per Taguchi's L9 orthogonal array, where variations in the TiO_2 weight%, normal load, and sliding speed were considered as the independent parameters. The influences of these parameters on the WR were determined through the analysis of variance (ANOVA) approach. After the wear tests, the sample surfaces were examined via OM.

3 Results and discussion

The mechanical, tribological, and microstructural characterizations of all the samples were performed, and the results were compared.

3.1 Mechanical characterizations

The flow curves for the AA6063, 99Al-1TiO_2, 97Al-3TiO_2, and 95Al-5TiO_2 samples are shown in Figure 5. The region of the flow curve up to the yield strength was considered as the linear elastic region, while the region after the yield strength and up to complete fracture was considered as the plastic region. Both regions are important for engineering design considerations. However, most designs are often developed by considering the linear elastic region as the limit. There were three samples each for the AA6063, 99Al-1TiO_2, 97Al-3TiO_2, and 95Al-5TiO_2 types that were subjected to uniaxial deformations. Hence, a total of 12 samples were tested to determine the σ_{ut}, σ_{ys}, microhardness, and percentage reduction in area at fracture. The standard deviations (STDVs) of these parameters are presented in Table 2.

The ultimate tensile strengths of all samples are shown in Figure 6. Considering plastic deformation, 95Al-5TiO_2 showed the highest ultimate tensile strength (σ_{ut}) of 253.20 N/mm^2 while the as-received AA6063 exhibited the lowest value (230.46 N/mm^2). The σ_{ut} value increased gradually with the weight% addition of TiO_2. It is seen that the coefficients of thermal expansion of TiO_2 and AA6063 are different from the dissimilar growths in their respective crystals during melting and solidification (Reddy et al., 2023); these dissimilar growths produce dislocations and substructures (Reed-Hill et al., 1973). The tensile load in the plastic region shows microvoids (generated during loading) that move and rearrange within the microstructure; whenever these microvoids reach the vicinities of localized TiO_2/dislocations, their mobilities/motions are hindered, which ultimately leads to the higher σ_{ut} (Dieter and Bacon, 1976). Hence, it is concluded that TiO_2

TABLE 2 Standard deviations of the σ_{ut}, σ_{ys}, microhardness, and percentage reductions in the areas at fractures for all samples.

Sample name	Stdev (σ_{ut})	Stdev (σ_{ys})	Stdev (microhardness)	Stdev (% reduction in area)
AA6063	3.03	1.84	1.49	0.24
99Al-1TiO_2	1.43	0.94	1.05	0.24
97Al-3TiO_2	0.88	0.69	1.55	0.21
95Al-5TiO_2	1.06	0.26	1.09	0.51

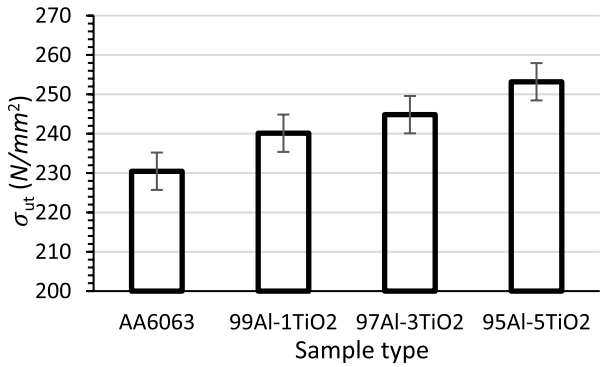

FIGURE 6
Ultimate tensile strengths of the AA6063, 99Al-1TiO_2, 97Al-3TiO_2, and 95Al-5TiO_2 samples.

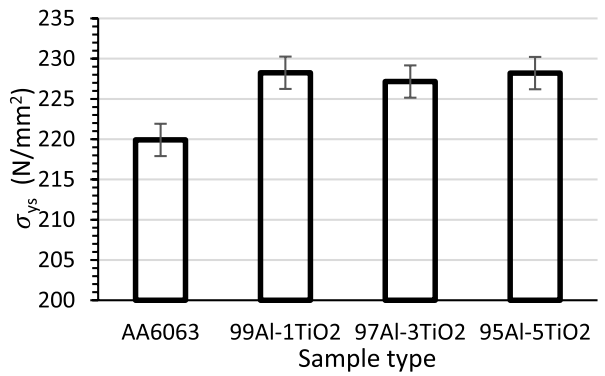

FIGURE 7
Yield strengths of the AA6063, 99Al-1TiO_2, 97Al-3TiO_2, and 95Al-5TiO_2 samples.

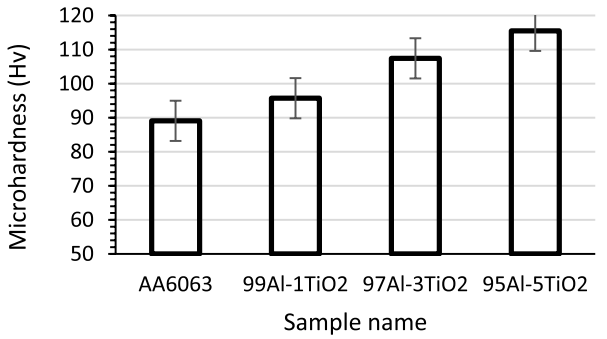

FIGURE 8
Microhardness of the AA6063, 99Al-1TiO_2, 97Al-3TiO_2, and 95Al-5TiO_2 samples.

provides the required dislocation strengthening responsible for the higher σ_{ut} (Dieter and Bacon, 1976). A similar hypothesis was reported by other researchers (Srivallirani and Rao, 2021; Reddy et al., 2023). The TiO_2 dislocation strengthening in the AA6063 matrix and grain refinement are yet to be confirmed from the microstructure. The higher strains (ϵ) in the AMMC samples than the as-received AA6063 indicate higher plastic strain, as shown in Figure 6; in other words, the addition of TiO_2 as the reinforcement enables the materials to accommodate higher strain energies. These higher strain energies provide the required driving forces to generate the dislocations and substructures (Reed-Hill et al., 1973; Anderson, 2017).

When considering linear elastic deformations, AA6063 showed the lowest yield strength (σ_{ys}) compared to the AMMC samples for all TiO_2 weight% values, as shown in Figure 7. The variations in σ_{ys} among the AMMC samples were minimal; in other words, the variations in weight% of TiO_2 significantly enhanced the ultimate tensile strengths but not the yield strengths. The minimal variations in σ_{ys} among the AMMC samples were compensated by shifts in the flow curves toward the strain axes (X-axis), as shown in Figure 5. In other words, the AMMC samples became less elastic as the shifts in the flow curves (up to the elastic limit) decreased the slopes of the stress–strain curves. The slope of the strain–strain curve indicates the elasticity, which is a material property independent of the shape and size. Hence, the AMMC samples had reduced stiffnesses with increasing weight% of added TiO_2.

According to the above observations, it is suggested that the addition of TiO_2 affected the plastic deformation characteristics significantly while the linear elastic characteristics remained almost similar. Therefore, the AMMC samples in the present work are more suitable for optimum designs based on their σ_{ut}. The microhardness values of the samples are presented in Figure 8, and these increased gradually with the addition of TiO_2. The 95Al-5TiO_2 sample showed the highest microhardness value (115.50 Hv), while the as-received AA6063 exhibited the lowest value (89.07 Hv); this suggests that the addition of TiO_2 provides the required precipitation strengthening, and similar observations have been reported by others (Kannan and Kishawy, 2006; Srivallirani and Rao, 2021). Increasing the σ_{ut} and ductility are challenges in designing AMMC materials. The percentage reductions in the areas at the fractures are shown in Figure 9. This area was largest for 95Al-5TiO_2, implying that the ultimate tensile strength and ductility were enhanced

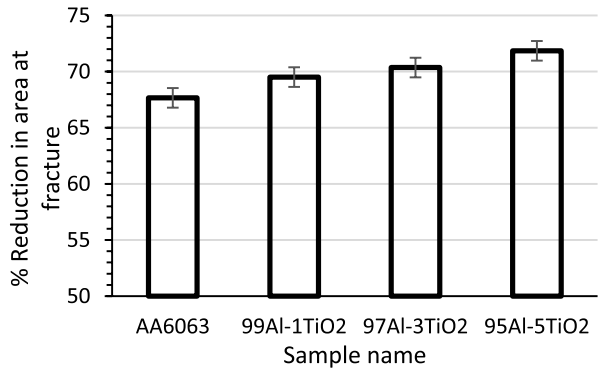

FIGURE 9
Percentage reductions in the areas at the fractures of the AA6063, 99Al-1TiO_2, 97Al-3TiO_2, and 95Al-5TiO_2 samples.

simultaneously with the addition of TiO_2; in other words, the ductility of the AMMCs increased without compromising the σ_{ut}. The values of percentage increases in the ultimate tensile strengths, yield strengths (σ_{ys}), microhardness, and percentage reductions in the areas at the fractures for the AMMC samples are presented in Table 3.

3.2 Tribological analyses and characterizations

The design of experiments (DOE) approach employing the Taguchi method of orthogonal arrays (L9, 3^3), was adopted to predict the WRs considering three different process parameters (Hendronursito et al., 2020), namely, TiO_2 weight%, normal load, and sliding speed. Accordingly, three levels were chosen for each of these three process parameters. The variance for WR is presented in Table 4; each row of the table represents the combination of parameters considered for the respective trial, and the last two rows indicate the residual errors and totals. The experimental data were analyzed using ANOVA to determine the effect of each parameter by considering the WR as the response. The ANOVA technique separated the observed variance data into different components for additional tests. An observed aggregate variability was grouped under two parts: systematic factors and random factors. The systematic factors had a statistical influence on the given dataset, whereas the random factors did not.

The F-statistic represents the ratio of mean-squares treatment to mean-squares error, while the *p*-value determines if the difference between the group means is statistically significant. The *p*-values of the individual parameters were significant at <0.05, indicating their statistical agreement. The contribution of the normal load was the highest, i.e., 53.72%, followed by those of the weight% of TiO_2 and sliding speed. The sliding speed had the least contribution among all parameters, i.e., 14.61%. The percentage contribution of the interaction effects between the normal load and weight% of TiO_2 was negligible.

Increasing values of the normal load on the pin increased the magnitude of contact stresses developed at the pin–disc interaction zone and dissipated the energy generated. The energy was dissipated in the form of heat via the force of contact friction and showed the surface damage. This suggests that the contact stresses affect the asperities on the disc surfaces, leading to ploughing. Subsequently, delamination along with severe plastic deformations were observed on the pin surfaces.

The current study examines the effects of TiO_2 addition to the AA6063 matrix; therefore, the wear surface was characterized using a load of 20 N and speed of 2 m/s. The wear surface of the as-received AA6063 sample is shown in Figure 10; this sample exhibited voids owing to particle pull-out during the wear test. Crack voids as microstructural features were also reported in a similar work by Bhoi and Singh (2023). The mechanically mixed layer was also observed in the microstructure. The wear surfaces of the 95Al-5TiO_2, 97Al-3TiO_2, and 99Al-1TiO_2 samples are shown in Figure 11, where microstructural features like voids, delamination, and microcracks are observed in the 95Al-5TiO_2 sample shown in Figure 11A. This suggests that the higher TiO_2 weight% causes matrix cracking and shearing of the cracks up to a certain extent. However, when the weight% of TiO_2 is decreased, the samples show wear debris in addition to voids and microcracks, as seen in Figures 11B,C. This suggests that the wear debris are caused by the abrasion and adhesion induced by sliding. Similar microstructural features like minor delamination and wear debris have also been reported in other works (Bhoi and Singh, 2023). The 95Al-5TiO_2 samples exhibited the least wear, while the AA6063 samples showed the most wear. It was observed that the WRs reduced with increasing weight% addition of TiO_2. Here, TiO_2 is a hard ceramic material; therefore, the addition of higher weight% of TiO_2 resists delamination and adhesive wear attributed to the ploughing effect caused by the pull-out particles. Hence, a significant decrease in the WR was observed for 95Al-5TiO_2. A higher percentage of reinforcement also improved the wear resistance of the aluminum matrix, suggesting that when the TiO_2 weight% was lower (1 and 3), the surface energy was also lower; this lower surface energy showed higher susceptibility to the wear force.

TABLE 3 Percentage increases in the ultimate tensile strengths, yield strengths, microhardness, and percentage reductions in the areas at fractures for the AMMC samples.

Sample name	% Increase in σ_{ut}	% Increase in σ_{ys}	% Increase in microhardness	% Reduction in area at fracture
99Al-1TiO_2	4.19	3.79	7.45	69.51
97Al-3TiO_2	6.24	3.30	20.60	70.36
95Al-5TiO_2	9.87	3.77	29.67	71.85

TABLE 4 Variances of the wear rate for different parameters.

Source	Degree of freedom	Sum of squares	Mean-variance	F-statistic	*p*-value	% of contribution
TiO_2 (weight %)	2	364.05	182.026	31.73	0.031	28.02
Load (*N*)	2	687.59	343.794	59.93	0.016	53.72
Speed (m/s)	2	195.32	97.659	17.02	0.055	14.61
Residual error	2	11.47	5.737	N/A	N/A	3.65
Total	8	1258.43	N/A	N/A	N/A	100.00

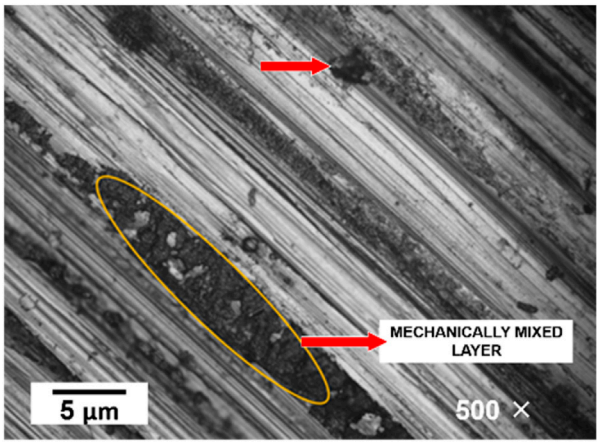

FIGURE 10
Optical microscopy image of the wear surface of AA6063, where the red arrow indicates voids caused by particle pull out.

The experimental trials for the wear tests were conducted in accordance with Taguchi's L9 orthogonal array, and the effects of the parameters on the WR were determined through ANOVA. The parameter levels considered in the trials are presented in Table 5. Furthermore, response surface plots (RSPs) were used to analyze the interaction effects of the parameters. The RSPs for different combinations of parameters are illustrated in Figure 12. Thus, reinforcing AA6063 with TiO_2 improves the wear resistances of the AMMCs.

3.3 Microstructural characterizations

3.3.1 Optical microscopy

The microstructure of the as-received AA6063 used as the matrix for all TiO_2 reinforcements is shown in Figure 13; the blue and green arrows indicate the grain boundaries (GBs) and dislocations/substructures at the grain interior, respectively. The grains were not equiaxed, meaning that they retained their thermal/mechanical strains during the thermal processing; furthermore, the presence of substructures was visible. This suggests that grain refinement may be achieved by the addition of TiO_2 as reinforcement; however, the extent of microstructural changes remains to be confirmed for the AMMC samples.

The OM-based microstructures of 99Al-1TiO_2, 97Al-3TiO_2, and 95Al-5TiO_2 are shown in Figure 14; the GBs and grain sizes are observed to decrease with the addition of TiO_2. The grain size was largest when the TiO_2 weight% was lowest, that is 1; this suggests that during melt solidification (cooling cycle), the grain growth was surpassed/pinned by the TiO_2 particles; in other words, the TiO_2 was an obstacle to grain growth, hence causing grain-size refinement. The strength of a material is evidenced by its microstructure, and a finer grain size indicates higher ultimate tensile strength. Therefore, it is suggested that the higher ultimate tensile strength (discussed in section 3.1) is achieved by the higher weight% of TiO_2. However, the presence of TiO_2 is yet to be confirmed from EDX characterizations.

3.3.2 EDX characterizations

The EDX images enable qualitative analyses of the 99Al-1TiO_2, 97Al-3TiO_2, and 95Al-5TiO_2 samples with different compositions,

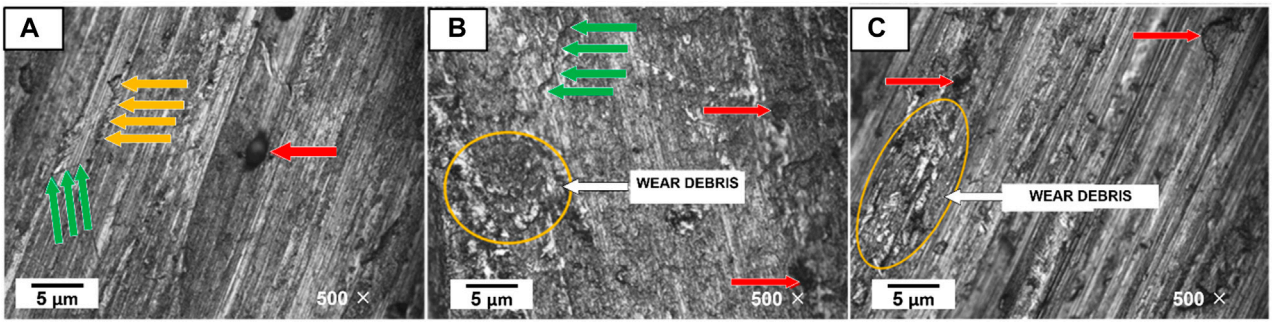

FIGURE 11
Optical microscopy images of the wear surfaces of the samples: **(A)** 95Al-5TiO_2, **(B)** 97Al-3TiO_2, and **(C)** 99Al-1TiO_2. The red arrow indicates voids caused by particle pull out, while the yellow and green arrows indicate delamination and microcracks, respectively.

TABLE 5 L9 orthogonal array for wear rate evaluations.

Trial no.	TiO_2 (wt%)	Load (*N*)	Speed (m/s)	Wear rate (mm^3/Nm)
1	1	10	1	42.11
2	1	15	2	54.12
3	1	20	3	76.67
4	3	10	1	34.01
5	3	15	2	50.32
6	3	20	3	51.32
7	5	10	1	38.65
8	5	15	2	40.22
9	5	20	3	50.96

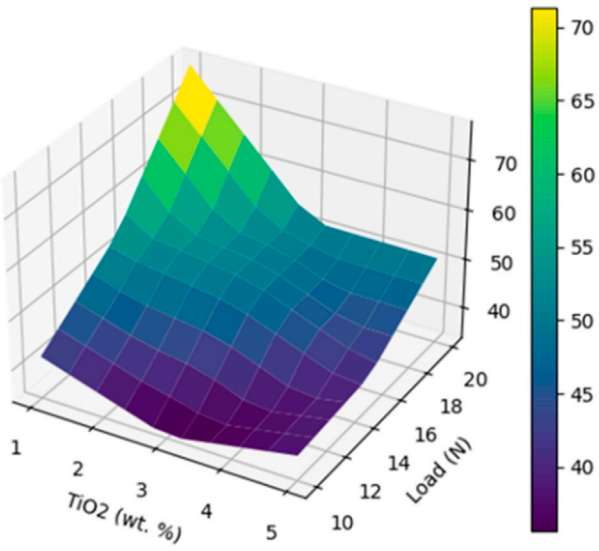

FIGURE 12
Effects of TiO_2 weight% and load on the wear rate.

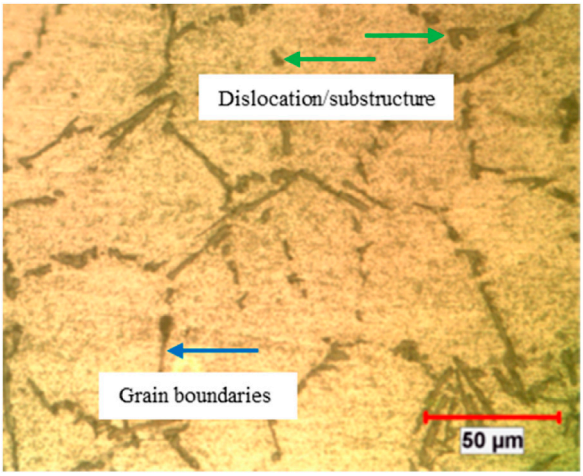

FIGURE 13
Optical microscopy image of AA6063 at a magnification of 500×. The blue and green arrows indicate the grain boundaries and dislocations/substructures in the grain interior, respectively.

as given in Figure 15. Elemental mapping was carried out at chosen areas of size ~400 µm × 400 µm in all samples; these areas are shown in the electron images given in Figures 15A–C. The elemental mappings of the samples confirm the presence of titanium (Ti) and oxygen (O) traces in the AA6063 matrix. The elemental maps of Ti originate from the K-shells (Ka1) of the samples, as shown in Figures 15D–F. Similarly, the elemental maps of O are shown in Figures 15G–I. From the elemental mapping, it was confirmed that TiO_2 was present in the AA6063 matrix. The dispersions of Ti observed in Figures 15D–F are in good agreement with the weight percentages of Ti added to the AA6063 matrix. The presence (violet-colored dots) of Ti is minimum in Figure 15D, corresponding with the lower Ti quantity of 1%, while the Ti presence is more prominent in Figure 15F, in which the Ti quantity was higher (5%). Furthermore, from Figures 15G–I, it is seen that O was not uniformly distributed, suggesting that most of the O atoms were bonded with Ti rather than Al. The corresponding quantitative EDX elemental weight% of the 99Al-1TiO_2, 97Al-3TiO_2, and 95Al-5TiO_2 samples are presented in Table 6. It is suggested that in addition to TiO_2, other reinforcements like boron carbide (B_4C) and silicon carbide (SiC) in the AMMCs can further influence the mechanical, tribological, and microstructural properties, which will be an investigation for a future work.

3.4 Microstructure–property correlations

The correlations between the microstructures and properties were analyzed by considering the influences of the grain sizes, microstructural features, and extent of inclusion of TiO_2 in the AA6063 matrix on the mechanical properties (ultimate tensile strength, yield strength, and microhardness). The Hall–Petch relationship depicts the relationship between the theoretical yield strength and grain size of a material (Reed-Hill et al., 1973; Dieter and Bacon, 1976; Armstrong, 2014):

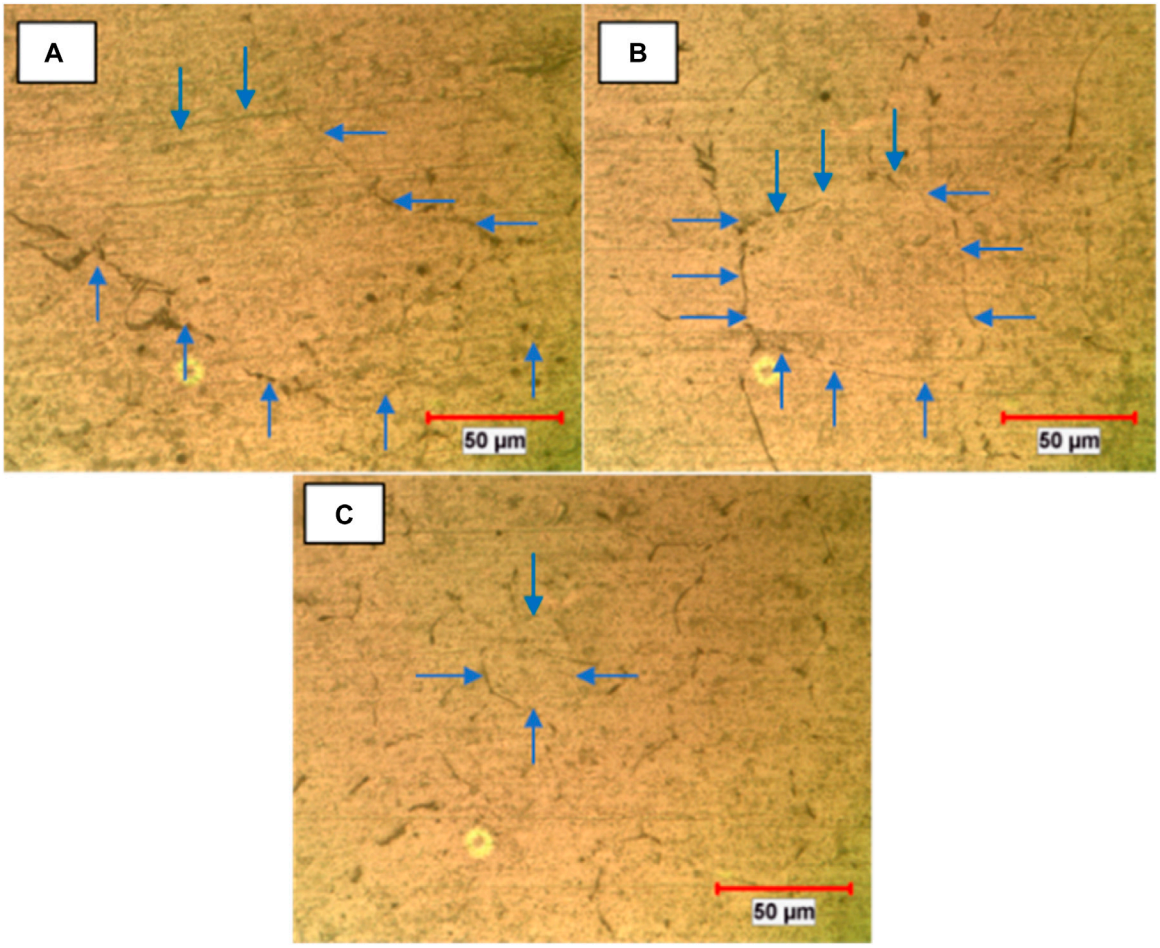

FIGURE 14
Optical microscopy images at a magnification of 500× for **(A)** 99Al-1TiO_2, **(B)** 97Al-3TiO_2, and **(C)** 95Al-5TiO_2. The blue arrows (in all figures) represent the grain boundaries.

TABLE 6 EDX elemental weight% of the 99Al-1TiO_2, 97Al-3TiO_2, and 95Al-5TiO_2 samples.

Element	99Al-1TiO_2		97Al-3TiO_2		95Al-5TiO_2	
	Weight (%)	Atomic (%)	Weight (%)	Atomic (%)	Weight (%)	Atomic (%)
B K	0	0	0	0	0	0
C K	8.79	17.52	10.87	20.43	12.39	22.79
O K	2.87	4.29	10.77	15.21	12.01	16.59
Al K	87.6	77.68	73.9	61.87	71	58.14
Si K	0.42	0.36	1.17	0.94	1.12	0.88
Ti K	0.32	0.16	3.29	1.55	3.47	1.6

$$\sigma_{ys} = \sigma_o + k_y d^{-0.5}, \quad (1)$$

where σ_{ys} and d are the yield strength and average grain diameter, respectively, while σ_o and k_y represent constants specific to a given material.

The above equation supports the hypothesis of a higher yield strength for a finer grain size as compared to coarse grains. In the present work, a similar trend was observed when the AMMC samples showed higher σ_{ys} values than AA6063 (Figure 7); in the context of the Hall–Petch relationship, the grain sizes of the

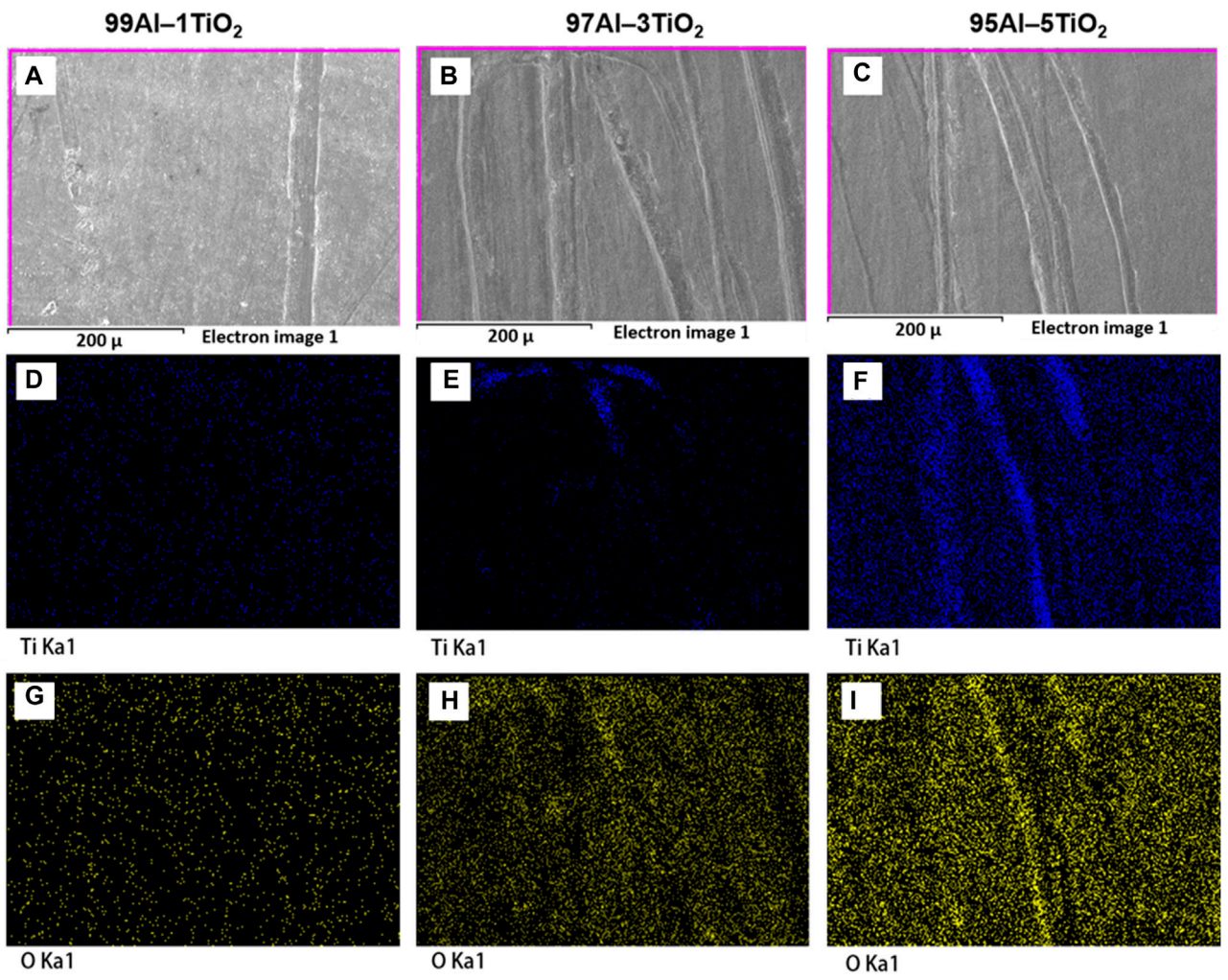

FIGURE 15
Scanning electron microscopy images showing the chosen areas for elemental mapping in the **(A)** 99Al-1TiO_2, **(B)** 97Al-3TiO_2, and **(C)** 95Al-5TiO_2 samples. Energy-dispersive X-ray spectroscopy images showing Ti distribution in the **(D)** 99Al-1TiO_2, **(E)** 97Al-3TiO_2, and **(F)** 95Al-5TiO_2 samples, as well as O distribution in the **(G)** 99Al-1TiO_2, **(H)** 97Al-3TiO_2, and **(I)** 95Al-5TiO_2 samples.

AMMC samples also reflect finer grains than AA6063. However, grain refinement to increase the ultimate tensile strength is a common heat-treatment process in physical metallurgy (Reed-Hill et al., 1973; Dieter and Bacon, 1976). The ultimate tensile strengths are higher for the AMMC samples than AA6063 (Figure 6); in addition, the hypothesis of a higher microhardness for a finer grain size was presented by other authors (Dieter and Bacon, 1976; Kannan and Kishawy, 2006). The present study depicts a similar trend for the microhardness. The 95Al-5TiO_2 sample showed the maximum microhardness value (115.50 Hv), whereas the AA6063 material exhibited the lowest value (89.07 Hv). The hypothesis of precipitation strengthening by TiO_2 was confirmed by EDX studies, as discussed in section 3.3.2. A similar hypothesis was reported in earlier works (Dieter and Bacon, 1976; Kannan and Kishawy, 2006). It is interesting to observe that the ductility of the AMMC increases without compromising the σ_{ut} in the present experimental route. In industries, it is often quite challenging to increase the mechanical properties of composites without compromising on the ductility and *vice versa*. Therefore, the current research has applications in manufacturing industries and material characterization laboratories.

Furthermore, the lower surface energy provides higher susceptibility against wear force. The addition of higher weight% of TiO_2 resisted matrix-reinforcement delamination and was attributed to the ploughing effect caused by the pull-out particles. Therefore, a substantial reduction in the WR was observed for 95Al-5TiO_2, as discussed in section 3.2. In addition to qualitative analysis of the microstructure, a quantitative analysis can be performed; this study establishes a more generalized relation between the grain sizes and yield strengths of the AMMC samples and AA6063. The Hall–Petch constants specific for a given TiO_2 weight% are also calculated. However, similar studies can be conducted for hybrid AMMCs by considering boron carbide as an additional reinforcement with TiO_2. The characterization techniques adopted in the present work can also be further improved by

calculating the different microstructural phase percentages using electron backscattered diffraction (EBSD).

4 Conclusion

The principal premises of the current research yield significant results as follows:

1. The σ_{ut} increases gradually with higher weight% addition of TiO_2; the 95Al-5TiO_2 sample shows the highest ultimate tensile strength (σ_{ut}) of 253.20 N/mm^2 while the as-received AA6063 exhibits the lowest value (230.46 N/mm^2).
2. When linear elastic deformation is considered, AA6063 shows the lowest yield strength (σ_{ys}) compared to the AMMC samples for all TiO_2 weight% values; however, the variations in σ_{ys} among the AMMC samples are minimal.
3. The microhardness of the samples increases gradually with the addition of TiO_2, and the percentage reduction in the area at the fracture is largest for 95Al-5TiO_2. The addition of TiO_2 as reinforcement enables the materials to accommodate higher strain energies. This higher strain energy provides the required driving force for the generation of dislocations and substructures, thereby increasing the microhardness with the addition of TiO_2.
4. The percentage contribution of normal load to the material wear is highest (53.72), followed by those of weight% of TiO_2 and sliding speed. The sliding speed has the least contribution among all parameters (14.61%). The percentage contribution of the interaction effects between normal load and weight% of TiO_2 are negligible.
5. Wear surface characteristics, such as microvoids, delamination, microcracks, and wear debris, are qualitatively observed for most of the samples to varying extents.
6. During melt solidification (cooling cycle), the grain growth is surpassed/pinned by the TiO_2 particles in the AMMCs; that is, TiO_2 hinders the grain growth, thereby providing grain-size refinement, which in turn provides a higher ultimate tensile strength.

Data availability statement

The original contributions presented in the study are included in the article/Supplementary Material; further inquiries can be directed to the corresponding authors.

Author contributions

JP: data curation, investigation, and writing–original draft. DR: conceptualization, methodology, supervision, and writing–review and editing. RM: formal analysis, software, and writing–review and editing. AK: formal analysis, investigation, and writing–review and editing. PK: formal analysis, investigation, and writing–review and editing. VHM: conceptualization, formal analysis, and writing–review and editing.

Funding

The author(s) declare that no financial support was received for the research, authorship, and/or publication of this article.

Conflict of interest

The authors declare that the research was conducted in the absence of any commercial or financial relationships that could be construed as a potential conflict of interest.

Publisher's note

References

Ahamad, N., Mohammad, A., Sadasivuni, K. K., and Gupta, P. (2020). Structural and mechanical characterization of stir cast Al–Al2O3–TiO2 hybrid metal matrix composites. *J. Compos. Mater.* 54 (21), 2985–2997. doi:10.1177/0021998320906207

Alagarsamy, S. V., and Ravichandran, M. (2019). Synthesis, microstructure and properties of TiO2 reinforced AA7075 matrix composites via stir casting route. *Mater. Res. Express* 6 (8), 086519. doi:10.1088/2053-1591/ab1d3b

Anderson, T. L. (2017). *Fracture mechanics: fundamentals and applications*. Boca Raton, FL: CRC Press.

Armstrong, R. W. (2014). Engineering science aspects of the Hall–Petch relation. *Acta Mech.* 225, 1013–1028. doi:10.1007/s00707-013-1048-2

Arsha, A. G., Manoj, V., Raag, L. A., Akhil, M. G., and Rajan, T. P. D. (2022). "Metallic nanocomposites for automotive applications," in *Nanotechnology in the automotive industry* (Elsevier), 163–198.

Bhoi, N. K., and Singh, H. (2023). Evaluation of susceptor-assisted microwave-sintering-produced Al-Y2O3 composite material's compression and reciprocating wear performance. *Phys. Scr.* 98 (10), 105938. doi:10.1088/1402-4896/acf744

Bhoi, N. K., Singh, H., Pratap, S., Gupta, M., and Jain, P. K. (2022a). Investigation on the combined effect of ZnO nanorods and Y2O3 nanoparticles on the microstructural and mechanical response of aluminium. *Adv. Compos. Mater.* 31 (3), 289–310. doi:10.1080/09243046.2021.1993555

Bhoi, N. K., Singh, H., Pratap, S., and Jain, P. K. (2022b). Aluminum yttrium oxide metal matrix composite synthesized by microwave hybrid sintering: processing, microstructure and mechanical response. *J. Inorg. Organomet. Polym. Mater.* 32, 1319–1333. doi:10.1007/s10904-021-02195-8

Chelladurai, S. J. S., Kumar, S. S., Venugopal, N., Ray, A. P., Manjunath, T., and Gnanasekaran, S. (2021). A review on mechanical properties and wear behaviour of aluminium based metal matrix composites. *Mater. Today Proc.* 37 (9), 908–916. doi:10.1016/j.matpr.2020.06.053

Dey, A., Shrivastav, M., and Kumar, P. (2021). Optimum performance evaluation during machining of Al6061/cenosphere AMCs using TOPSIS and VIKOR based multi-criteria approach. *Proc. Institution Mech. Eng. Part B J. Eng. Manuf.* 235 (13), 2174–2188. doi:10.1177/0954405420958770

Dieter, G. E., and Bacon, D. (1976). *Mechanical metallurgy*, 3. New York: McGraw-Hill, 43–53.

Dutt, A. K., Sindhuja, K., Reddy, S. V. N., and Kumar, P. (2021). "Application of artificial neural network to friction stir welding process of AA7050 aluminum alloy," in *Advances in industrial automation and smart manufacturing: select proceedings of ICAIASM 2019* (Singapore: Springer), 407–414.

Goyat, V., Ghangas, G., Sirohi, S., Kumar, A., and Nain, J. (2022). A review on mechanical properties of coir based composites. *Mater. Today Proc.* 62 (Part 4), 1738–1745. ISSN 2214-7853. doi:10.1016/j.matpr.2021.12.252

Hang, Z. Y. (2022). *Additive friction stir deposition*. Elsevier.

Hendronursito, Y., Rajagukguk, T. O., Safii, R. N., Sofii, A., Isnugroho, K., Birawidha, D. C., et al. (2020). Analysis of aluminium basalt particulate composite using stirring casting method through taguchi method approach. *IOP Conf. Ser. Mater. Sci. Eng.* 807 (1), 012003. doi:10.1088/1757-899x/807/1/012003

Joshua, K. J., Vijay, S. J., and Selvaraj, D. P. (2018). Effect of nano TiO2 particles on microhardness and microstructural behavior of AA7068 metal matrix composites. *Ceram. Int.* 44 (17), 20774–20781. doi:10.1016/j.ceramint.2018.08.077

Kannan, S., and Kishawy, H. A. (2006). Surface characteristics of machined aluminium metal matrix composites. *Int. J. Mach. Tools Manuf.* 46 (15), 2017–2025. doi:10.1016/j.ijmachtools.2006.01.003

Kardak, A. A., and Sinclair, G. B. (2020). Stress concentration factors for ASTM E8/E8M-16a standard round specimens for tension testing. *J. Test. Eval.* 48 (1), 711–719. doi:10.1520/jte20190549

Kumar, P. (2022). Fatigue life estimation of 7020 aluminum alloy subjected to aqueous sodium chloride solution. *Key Eng. Mater.* 928, 17–23. doi:10.4028/p-oi3mxu

Kumar, P., Hussain, S. S., Kumar, A., Srivastava, A. K., Hussain, M., and Singh, P. K. (2024). "10 Finite element method investigation on delamination of 3D printed hybrid composites during the drilling operation," in *3D printing technologies: digital manufacturing, artificial intelligence, industry 4.0*. Editors A. Kumar, P. Kumar, N. Sharma, and A. Kumar Srivastava (Berlin, Boston: De Gruyter), 223–234. doi:10.1515/9783111215112-010

Kumar, P., and Verma, B. B. (2022). Propagation of corrosion induced fatigue crack in aluminum alloy. *AIMS Mater. Sci.* 9 (3), 512–521. doi:10.3934/matersci.2022030

Kumar Bhoi, N., Singh, H., and Pratap, S. (2020). Synthesis and characterization of zinc oxide reinforced aluminum metal matrix composite produced by microwave sintering. *J. Compos. Mater.* 54 (24), 3625–3636. doi:10.1177/0021998320918646

Manojkumar, M., and Shanmuga Prakash, R. (2016). Wear characteristics of hybrid Al 6063 matrix composites reinforced with graphite and fly ash particulates. *Appl. Mech. Mater.* 854 (January), 1–9. doi:10.4028/www.scientific.net/amm.854.1

Mavhungu, S. T., Akinlabi, E. T., Onitiri, M. A., and Varachia, F. M. (2017). Aluminum matrix composites for industrial use: advances and trends. *Procedia Manuf.* 7, 178–182. doi:10.1016/j.promfg.2016.12.045

Nandyala, K., Kumar, B. S., and Durga Bhavani, G. I. K. (2023). Developing of hybrid composite of Al-6068 and Al-7075 by reinforcing TiO2/BN by stir casting process and finding mechanical and wear behavior of the hybrid composition. *Chem. Bull.* 2023 (6), 1036–1044. doi:10.31838/ecb/2023.12.6.95

Pramanik, A. (2016). Effects of reinforcement on wear resistance of aluminum matrix composites', *Transactions of Nonferrous Metals Society of China (English Edition). Nonferrous Metals Soc. China* 26 (2), 348–358. doi:10.1016/S1003-6326(16)64125-0

Ramesh, B. T., Kumar, B. A. M., and Swamy, R. P. (2015). Dry sliding wear test conducted on pin-on-disk testing setup for Al6061-sic metal matrix composites fabricated by powder metallurgy. *Int. J. Innovative Sci. Eng. Technol.* 2 (6).

Reddy, D. A. K., Rajesh, G., Anbuchezhiyan, G., Ponshanmugakumar, A., Ganesan, R., Latha, A., et al. (2023). Investigating the mechanical properties of titanium dioxide reinforced magnesium composites. *Mater. Today Proc.* doi:10.1016/j.matpr.2023.05.193

Reddy, K. S. K., Lekha, B. C., Sakshi, K. U., Chouhan, M. S., Karthikeyan, R., and Aparna, S. (2022). Effect of different reinforcements on aluminium composite properties–a review. *Mater. Today Proc.* 62, 3963–3967. doi:10.1016/j.matpr.2022.04.572

Reed-Hill, R. E., Abbaschian, R., and Abbaschian, R. (1973). *Physical metallurgy principles*, 17. New York: Van Nostrand.

Shin, J. H., Choi, H. J., Cho, M. K., and Bae, D. H. (2014). Effect of the interface layer on the mechanical behavior of TiO2 nanoparticle reinforced aluminum matrix composites. *J. Compos. Mater.* 48 (1), 99–106. doi:10.1177/0021998312469238

Shuvho, M. B. A., Chowdhury, M. A., Kchaou, M., Roy, B. K., Rahman, A., and Islam, M. A. (2020). Surface characterization and mechanical behavior of aluminum based metal matrix composite reinforced with nano Al2O3, SiC, TiO2 particles. *Chem. Data Collect.* 28, 100442. doi:10.1016/j.cdc.2020.100442

Singh, A., Srivastava, A. K., Singh, G., Singh, A. D., Singh, H. K., Kumar, A., et al. (2023). Utilization of plastic waste for developing composite bricks and enhancing mechanical properties: a review on challenges and opportunities. *Adv. Polym. Technol.* 2023, 1–24. Article ID 6867755, 24 pages. doi:10.1155/2023/6867755

Srivallirani, K., and Rao, M. V. (2021). Fabrication and mechanical characterization of Al 7050/TiO2/BN hybrid metal matrix composites. *Mater. Today Proc.* 39, 1750–1753. doi:10.1016/j.matpr.2020.06.386

Srivyas, P. D., and Charoo, M. S. (2019). Application of hybrid aluminum matrix composite in automotive industry. *Mater. Today Proc.* 18, 3189–3200. doi:10.1016/j.matpr.2019.07.195

Subramanian, K., Murugesan, S., Mohan, D. G., and Tomków, J. (2021). Study on dry sliding wear and friction behaviour of al7068/si3n4/bn hybrid composites. *Materials* 14 (21), 6560. doi:10.3390/ma14216560

Tyagi, A., Pandey, S. M., Walia, R. S., Murtaza, Q., and Kumar, A. (2021). "Effect of temperature on the sliding wear behavior of HVOF sprayed Al_2O_3 composite coating," in *Advances in materials and mechanical engineering. Lecture notes in mechanical engineering*. Editors C. Pandey, V. Goyat, and S. Goel (Singapore: Springer). doi:10.1007/978-981-16-0673-1_3

Veeresh Kumar, G. B., Gouda, P. S. S., Pramod, R., and Rao, C. S. P. (2017). Synthesis and characterization of TiO2 reinforced Al6061 composites. *Adv. Compos. Lett.* 26 (1), 096369351702600–096369351702623. doi:10.1177/096369351702600104

Wagih, A., Junaedi, H., Mahmoud, H. A., Lubineau, G., Kumar, A., and Sebaey, T. A. (2024). Enhanced damage tolerance and fracture toughness of lightweight carbon-Kevlar fiber hybrid laminate. *J. Compos. Mater.* 0 (0), 1109–1121. doi:10.1177/00219983241235853

Yunus, M., and Alfattani, R. (2023). Assessment of mechanical and tribological behavior of AA6061 reinforced with B4C and gr hybrid metal matrix composites. *Coatings* 13 (9), 1653. doi:10.3390/coatings13091653